



# Structural Features and Digestibility of Corn Starch With Different Amylose Content

Xinxin Lv<sup>1,2</sup>, Yan Hong<sup>1,2,3,4\*</sup>, Qiwei Zhou<sup>2</sup> and Chengchen Jiang<sup>2</sup>

<sup>1</sup> Key Laboratory of Synthetic and Biological Colloids, Ministry of Education, Wuxi, China, <sup>2</sup> School of Food Science and Technology, Jiangnan University, Wuxi, China, <sup>3</sup> Qingdao Special Food Research Institute, ChangCheng Avenue, Qingdao, China, <sup>4</sup> Collaborative Innovation Center for Food Safety and Quality Control, Jiangnan University, Wuxi, China

## OPEN ACCESS

### Edited by:

Tao Feng,  
Shanghai Institute of  
Technology, China

### Reviewed by:

Zhang Yayuan,  
Guangxi Academy of Agricultural  
Science, China  
Xiaozhi Tang,  
Nanjing University of Finance and  
Economics, China

### \*Correspondence:

Yan Hong  
hongyan@jiangnan.edu.cn

### Specialty section:

This article was submitted to  
Food Chemistry,  
a section of the journal  
Frontiers in Nutrition

Received: 09 April 2021

Accepted: 30 April 2021

Published: 21 June 2021

### Citation:

Lv X, Hong Y, Zhou Q and Jiang C  
(2021) Structural Features and  
Digestibility of Corn Starch With  
Different Amylose Content.  
Front. Nutr. 8:692673.  
doi: 10.3389/fnut.2021.692673

In this study, the *in vitro* digestibility of corn starch with different amylose content was determined. The results showed that waxy corn starch (WCS) and corn starch (CS) have the highest digestibility, while high amylose corn starch (HACS) has a higher content of resistant starch (RS). Besides being related to amylose content, RS content is also closely related to particle shape, debranched fine structure, molecular structure, and semi-crystalline structure. HACS can maintain a complete particle structure after gelatinization and enzymolysis; differential scanning calorimetry showed a positive correlation between gelatinization enthalpy and RS content. As the amylose content increased, the content of *fa* (DP 6–12) decreased, while the content of *fb2* (DP 25–36) and *fb3* (DP  $\geq$  37) increased, which in-turn decreased the cluster polymer formed by short branch chains, and the formation of more hydrogen bonds between long chain branches improved starch stability. D, which characterizes the compactness of starch semi-crystalline structure, increased with the increase of RS content. HACS 60 with the highest RS content had a unique surface fractal structure between  $7.41 < d (2\pi/q) < 10.58$  nm, indicating that the dense structure is effective in maintaining the RS content.

**Keywords:** *in vitro* digestibility, amylose, chain length distribution, crystal structure, corn starch

## INTRODUCTION

Starch is one of the most important carbohydrates in human life, with different applications in industries such as the food, petroleum, pharmaceutical, paint, and cosmetic industries, among others (1). Corn is the main botanical origin of starch production (2). Starch comprises three parts: rapidly digestible starch (RDS), slowly digestible starch (SDS), and resistant starch (RS) (3). RDS leads to a rapid increase in blood glucose levels after meals, which is harmful to diabetics; SDS releases glucose slowly, which can maintain stable blood glucose levels after meals. RS cannot be digested by enzymes in the small intestine, but can be fermented by microorganisms to produce short-chain fatty acids to promote beneficial intestinal flora and human health (4). Therefore, reducing the digestibility of starch is an effective strategy to prevent and control chronic diseases such as diabetes and obesity (5).

RS has been classified into five general subtypes: RS1–RS5 (6). Different types of RS have different mechanisms, RS2 refers to natural resistant starch granules such as high amylose corn starch (HACS), raw potato, and banana starch. HACS is of interest because of its health benefits and industrial uses (7). Understanding the resistance mechanism of HACS is an important step

to regulate RS content. To the best of our knowledge, the structural features of starch that resist the action of digestive enzymes mainly include starch granules compactness, amylopectin/amylose ratio, amylopectin fine structures, molecular structure, crystalline structure, and semi-crystalline lamellae (8–13). Amylose can span the crystalline and amorphous regions of starch and connect the inside and outside of the granule. The high amylose content in HACS causes starch to form tightly packed granules inaccessible to digestive enzymes (14). The higher the amylose content, the more conducive is the formation of tightly arranged linear sequences, thereby reducing the damage to starch structure by heat treatment and reducing the rate of starch enzymatic hydrolysis (15, 16). To improve the starch resistance of HACS, researchers increased the amylose content through genetic breeding, and to change the amylose arrangement (17). The increase in amylose content will also bring about other structural changes. The effect of the fine structure of amylose on the function of HACS has been studied, and the molecular structure of starch is also very important to its overall physical and chemical properties. In the debranched chain length distributions, a higher proportion of long chains ( $DP \geq 37$ ) will increase the starch gelatinization temperature and reduce the peak viscosity (18, 19). However, short chains ( $DP 6-12$ ) may cause imperfections by formation of crystallites. Starch with fewer short chains has better enzymatic resistance and heat stability. Small angle X-ray scattering (SAXS) analysis has been widely used to study the semi-crystalline structure of starches from different sources (12, 20–22) and different modified starches (23–25). The rapid development of SAXS analysis technology provides more possibilities for studying the semi-crystalline structure of HACS. The closer the semi-crystalline structure, the higher the thermal stability and resistance to the enzymatic degradation of starch.

HACS has always been an important RS, but the principle of amylose increasing starch RS content needs further study. This experiment studied the changes in particle shape, molecular structure, crystal structure and fractal structure brought about by amylose, and its influence on RS content. The results obtained from these studies were used to establish the correlation between structural features and *in vitro* digestibility, provide accurate target structures for gene breeding, and reduce the difficulty of gene breeding to regulate the RS content of corn starch.

## MATERIALS AND METHODS

### Materials

Waxy corn starch (WCS, moisture content: 12.98%, amylose content: 3.23%) was purchased from COFCO Corporation (Jilin, China); Corn starch (CS, moisture content: 11.95%, amylose content: 20.13%), HACS 70 (moisture content: 13.09%, amylose content: 71.16%), and HACS 80 (moisture content: 12.38%, amylose content: 80.71%) were purchased from AnHui King Corn Agriculture Science and Technology Development Co., Ltd. (Anhui, China); HACS 50 (moisture content: 12.78%, amylose content: 51.22%) was purchased from Cargill Investment Co., Ltd. (Shanghai, China); HACS 60 (moisture content: 9.42%, amylose content: 61.26%) was purchased from Yiruiian Food

Ingredients Co., Ltd. (Shanghai, China); Pancreatin (porcine pancreas,  $8 \times USP$ ), amyloglucosidase (*Aspergillus niger*,  $\geq 300$  U/mL), pepsin (porcine stomach mucosa,  $\geq 250$  U/mg), invertase (solids,  $\geq 300$  U/mg), and isoamylase (protein,  $3 \times 10^6$  U/mg) were purchased from Sigma-Aldrich (St. Louis, MI, USA); The glucose oxidase-peroxidase (GOPOD) kit was purchased from Beijing Leadman Biochemistry Co., Ltd. (Beijing, China); Other reagents were purchased from China National Medicines Co., Ltd. (Shanghai, China) and were of analytical grade.

### *In vitro* Digestibility

The method for determining the digestibility of starch is based on previous studies (3, 26). The released glucose content was measured using a GOPOD kit and calculated using Eq. (1):

$$\text{glucose\%} = \frac{(A_t - A_b) \times c \times V \times D}{A_s \times w} \times 100 \quad (1)$$

Where  $A_t$  is the absorbance of the test solution at 520 nm;  $A_b$  is the absorbance of the blank solution at 520 nm;  $c$  is the concentration of the standard solution (mg glucose/mL, provided by the glucose oxidase-peroxidase kit);  $V$  is the total volume of the test solution;  $D$  is the dilution factor;  $A_s$  is the absorbance of the standard solution at 520 nm;  $w$  is the weight of the sample used for analysis (mg), which can be corrected for moisture content using Eqs. (2)–(4).

$$RDS = (G20 - FG) \times 0.9 \quad (2)$$

$$SDS = (G120 - G20) \times 0.9 \quad (3)$$

$$RS = TS - RDS - SDS \quad (4)$$

Where FG is the free glucose content and TS is the total starch content (% dry basis) of the sample.

### Polarizing Microscopy Analysis

Samples (0.2 mg, dry basis) were weighed, 2 mL of water was added, and the samples were gelatinized at 100°C for 30 min. The gelatinized samples were freeze-dried and dispersed in an aqueous solution (glycerin:water = 1:1). The polarized light birefringence cross was observed under a polarized light microscope (Olympus, Tokyo, Japan).

### Scanning Electron Microscopy

After the starch is gelatinized at 100°C, simulated digestion *in vitro* was performed. The products digested for 120 min were collected, ethanol precipitated and freeze-dried. According to the reported method (27), the corn starch with different amylose content and the collected digestion products were fixed and sprayed with gold, and the samples were observed and photographed under an acceleration voltage of 3 kV.

### Rapid Viscosity Analysis

The pasting properties of the HACS were determined by rapid viscosity analysis (RVA) using a Tech Master analyzer (23) (Perten, Stockholm, Sweden). Each complex was suspended in deionized water (10%, w/w, dry basis) in an RVA aluminum box, the samples were heated from 50 to 140°C in 9 min, then kept at 140°C for 2 min, and finally dropped from 140 to 50°C in 9 min.

## Differential Scanning Calorimetry

The thermal properties were determined by differential scanning calorimetry (DSC) using the method already reported (28). The temperature range was 50–160°C, and the heating rate was 10°C/min.

## Debranched Chain Length Distributions

The debranched chain length distributions of samples were determined using the method already reported (29), with some modifications. Samples (10 mg, dry basis) were dissolved in 2 mL citrate-disodium hydrogen phosphate buffer solution (pH = 3.5) and gelatinized at 100°C for 30 min. After the solution was cooled to 40°C, 100 µL isoamylase solution was added, and the reaction was conducted for 24 h at 40°C. The reaction was stopped by incubating for 20 min in a boiling water bath. Samples were then allowed to cool to room temperature and centrifuged at 13,000 g for 10 min. The supernatants were filtered through a 0.45 mm nylon microporous membrane to measure the chain length distributions using High Performance Anion Exchange Chromatography-Pulsed Amperometric Detector (Thermo, Waltham, Massachusetts, USA).

## Gel Permeation Chromatography

The weight-average molecular weight of the samples were measured using gel permeation chromatography (GPC) according to a previous method (30). After peak fitting, GPC data were used to characterize the weight-average molecular weight ( $M_w$ ) of the samples.

## X-Ray Diffraction

According to the method already reported (31), the crystal structure was determined using an X-ray diffractometer (Bruker AXS Ltd., Leipzig, Germany), and the relative crystallinity was calculated using the MDI Jade 5.0 software.

## Small Angle X-Ray Scattering Analysis

The semi-crystalline structure was determined by Small angle X-ray scattering (SAXS) analysis (32). SAXS measurements were conducted on SAXSess small angle X-ray scattering system (Anton Paar, Graz, Austria) which was equipped with a PW3830 X-ray generator (PANalytical) using Cu K $\alpha$  radiation ( $\lambda = 0.1542$  nm).

## Statistical Analysis Methods

The data were statistically analyzed using IBM SPSS Statistics v20 software (IBM, Armonk, NY, USA). Results were expressed as mean  $\pm$  standard deviation.

## RESULTS AND DISCUSSION

### *In vitro* Digestibility

The results of the *in vitro* digestive properties of corn starch with different amylose content are shown in **Figure 1**. During the 150 min digestion process, according to the slope of the glucose release curves, samples were all digested rapidly within 20 min of enzymatic hydrolysis, whereas the digestion rate within 20–150 min increased slowly. The *in vitro* digestibility of HACS ranged from 45 to 80%, indicating that HACS has strong digestion resistance. The RS content values of RDS, SDS, and RS

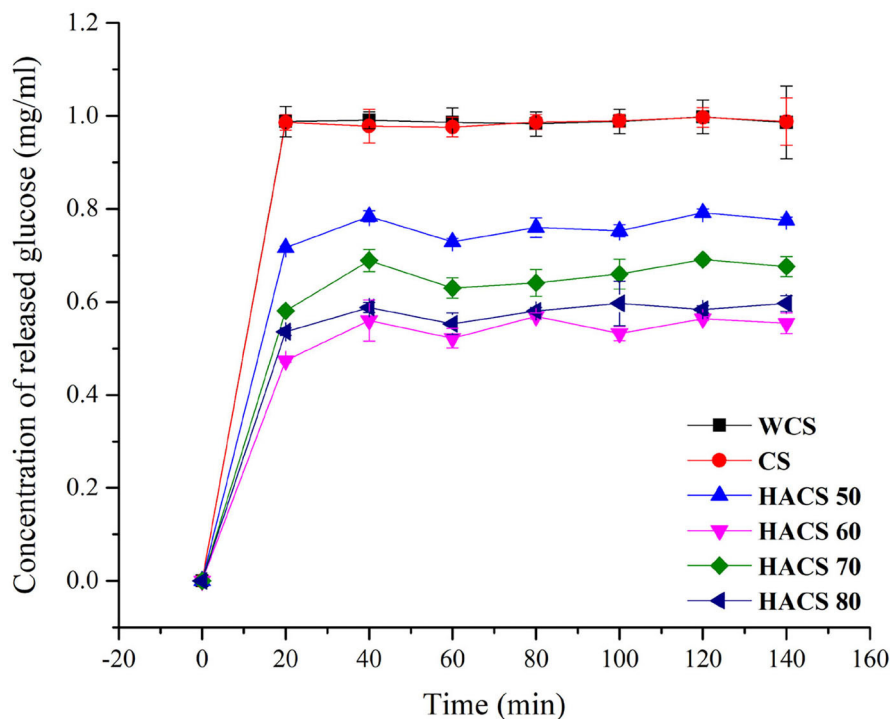


**FIGURE 1** | *In vitro* digestibility of corn starch with different amylose content.

for the samples are listed in **Table 1**. The RDS content of WCS and CS was  $\sim 88\%$ . In comparison, the HACS with over 50% amylose content showed higher RS content. With the increase in amylose content, the RS content of HACS 50, HACS 70, and

HACS 80 also gradually increased. There is a positive correlation between amylose content and RS content (33), which is mainly because amylose is not easily digested by enzymes (34).

It is worth noting that the sample with the highest RS content is HACS 60, which has an RS content of 49.10%. This result shows that besides the amylose content, some factors affect the RS content of starch (9). When determining starch digestibility, researchers found HACS retains some intact granules after gelatinization. Therefore, to further explore the factors affecting the RS content, gelatinized HCAS particles were observed.

**TABLE 1** | RDS, SDS, RS content of corn starch with different amylose content.

| Samples | RDS (%)                       | SDS (%)                      | RS (%)                        |
|---------|-------------------------------|------------------------------|-------------------------------|
| WCS     | 88.92 $\pm$ 0.83 <sup>e</sup> | 1.80 $\pm$ 0.08 <sup>a</sup> | 9.28 $\pm$ 0.75 <sup>b</sup>  |
| CS      | 88.74 $\pm$ 0.47 <sup>e</sup> | 3.49 $\pm$ 0.13 <sup>b</sup> | 7.01 $\pm$ 0.34 <sup>a</sup>  |
| HACS 50 | 65.00 $\pm$ 0.23 <sup>d</sup> | 6.64 $\pm$ 0.39 <sup>d</sup> | 28.35 $\pm$ 0.17 <sup>c</sup> |
| HACS 60 | 43.76 $\pm$ 0.76 <sup>a</sup> | 7.13 $\pm$ 0.45 <sup>d</sup> | 49.10 $\pm$ 0.31 <sup>f</sup> |
| HACS 70 | 52.13 $\pm$ 0.24 <sup>c</sup> | 9.47 $\pm$ 0.40 <sup>e</sup> | 38.40 $\pm$ 0.18 <sup>d</sup> |
| HACS 80 | 48.38 $\pm$ 0.31 <sup>b</sup> | 4.28 $\pm$ 0.24 <sup>c</sup> | 47.34 $\pm$ 0.14 <sup>e</sup> |

Values followed by different superscripts in the same column are significantly different ( $p < 0.05$ ).

## Particle Integrity

### Cross-Polarization

The orderly arranged starch molecules of crystalline regions and disorderly arranged starch molecules in amorphous regions normally generate an anisotropic phenomenon in starch granules, leading to a birefringence cross under polarized

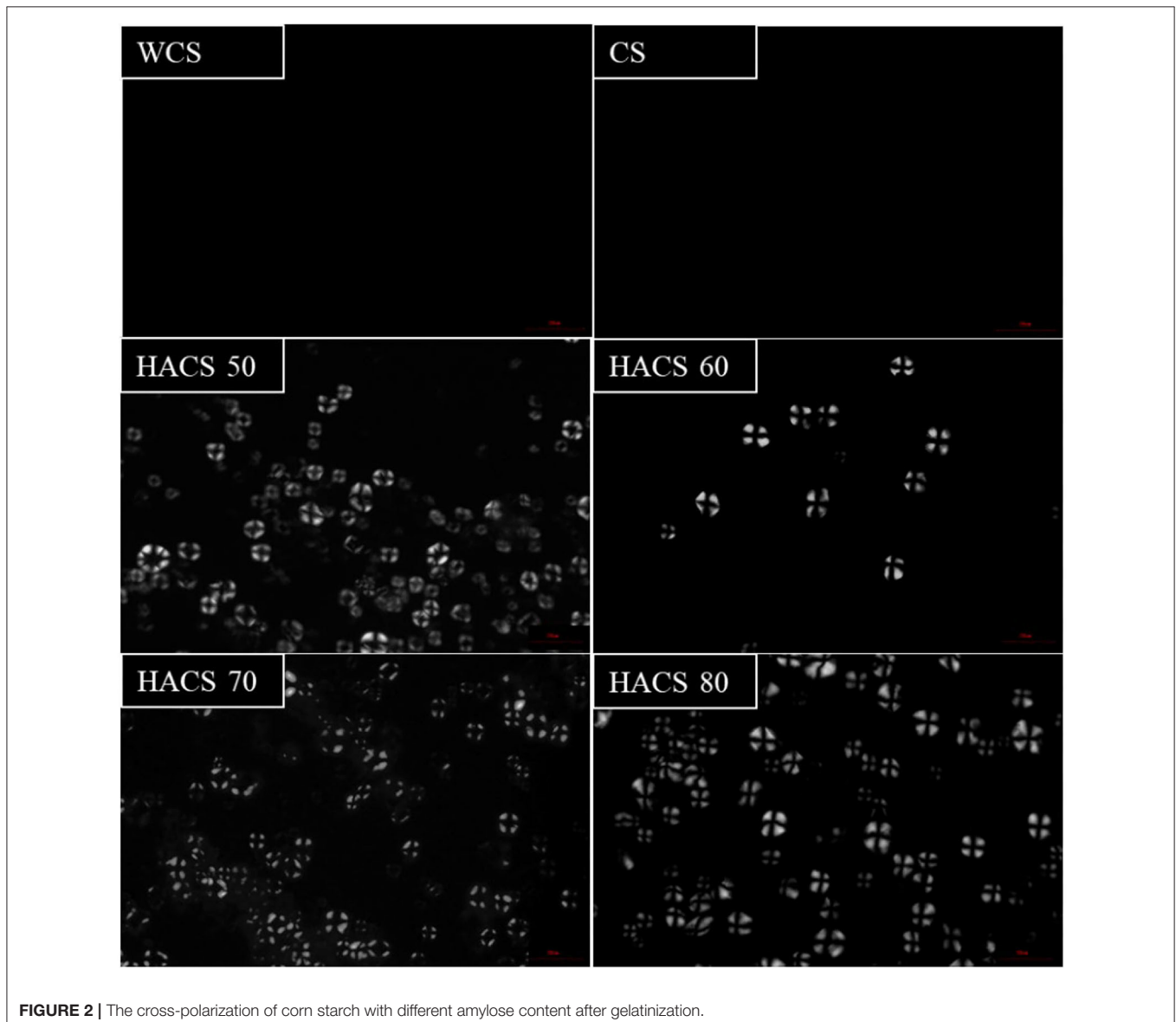


**FIGURE 2** | The cross-polarization of corn starch with different amylose content after gelatinization.

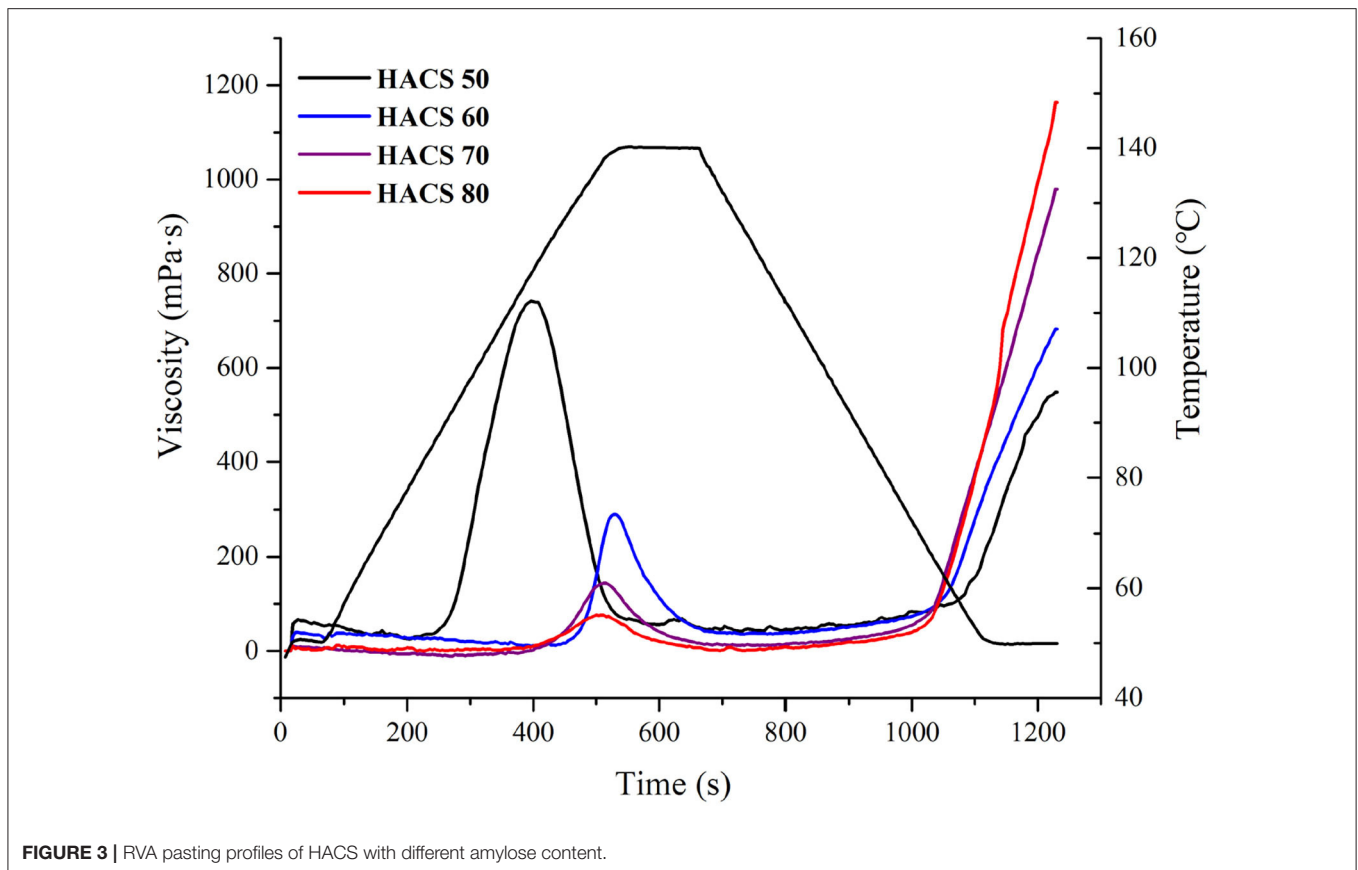


**FIGURE 3** | RVA pasting profiles of HACS with different amylose content.

**TABLE 2** | Gelatinization characteristic value of corn starch with different amylose content.

| Samples | Peak viscosity (mPa·s)    | Breakdown (mPa·s)         | Final viscosity (mPa·s)   | Setback (mPa·s)         |
|---------|---------------------------|---------------------------|---------------------------|-------------------------|
| WCS     | 3507.7 ± 1.5 <sup>f</sup> | 2455.7 ± 1.5 <sup>f</sup> | 1487.0 ± 1.0 <sup>e</sup> | 154 ± 1.0 <sup>a</sup>  |
| CS      | 3356.7 ± 2.1 <sup>e</sup> | 1258.3 ± 1.5 <sup>e</sup> | 3927.0 ± 1.7 <sup>f</sup> | 434 ± 0.6 <sup>b</sup>  |
| HACS 50 | 741.6 ± 1.5 <sup>d</sup>  | 699.7 ± 1.5 <sup>d</sup>  | 548.0 ± 2.0 <sup>a</sup>  | 506 ± 1.2 <sup>c</sup>  |
| HACS 60 | 290.0 ± 1.0 <sup>c</sup>  | 278.3 ± 0.6 <sup>c</sup>  | 681.0 ± 1.0 <sup>b</sup>  | 670 ± 0.5 <sup>d</sup>  |
| HACS 70 | 144.0 ± 1.0 <sup>b</sup>  | 132.0 ± 1.0 <sup>b</sup>  | 978.7 ± 1.5 <sup>c</sup>  | 967 ± 1.0 <sup>e</sup>  |
| HACS 80 | 76.4 ± 0.5 <sup>a</sup>   | 76.2 ± 1.3 <sup>a</sup>   | 1164.3 ± 1.5 <sup>d</sup> | 1163 ± 2.1 <sup>f</sup> |

Values followed by different superscripts in the same column are significantly different ( $p < 0.05$ ).

light (35). The gelatinized corn starch granules with different amylose content were analyzed (Figure 2). Figure 2 shows that after gelatinization, HACS still maintains cross-polarization, indicating that the internal structure of the starch granules with an amylose content >50% [meet the definition of high amylose starch (7)] was tight, and the arrangement of amylose and amylopectin was not completely destroyed. The internal structure of HACS was compact and could refrain the particles from breaking under high temperature, and would reduce the water holding capacity of starch, thus reducing the viscosity of starch after gelatinization and starch RDS content. Therefore, the gelatinization properties of HACS were measured.

### Rapid Viscosity Analysis of Pasting Properties

Under excessive water environment and heating conditions, starch granules swell and rupture after being absorbed by water, causing the viscosity of the sample to increase. Observing the starch gelatinization process helps to understand the breakdown of starch granules (36). As seen in Figure 3, the peak viscosity of HACS decreased with an increase in the amylose content, which indicates that increased amylose content makes it more difficult for the granules to break (37). This result is consistent with the cross-polarization after HACS gelatinization. Setback viscosity indicates starch retrogradation during the cooling period, and the final viscosity reflects the viscosity of cold starch paste, both of which increased with the increase in amylose content (Table 2); HACS 80 had the highest final (1,164 mPa·s) and setback (1,163 mPa·s) viscosities.

### Starch Granules

It can be seen from Figures 4A–F that the WCS and CS particles are polygonal, while HACS has some spherical granules and rod/filamentous granules, which is consistent with previous reports (38). The granular structure of HACS granules contributed to the resistance of starch molecules to pancreatic  $\alpha$ -amylase hydrolysis. Amylose increases the tightness of starch granules, so starch granules still exist after HACS enzymatic hydrolysis for 120 min (Figures 4G–L), while WCS and CS can only observe broken gel pieces. This is mainly due to the

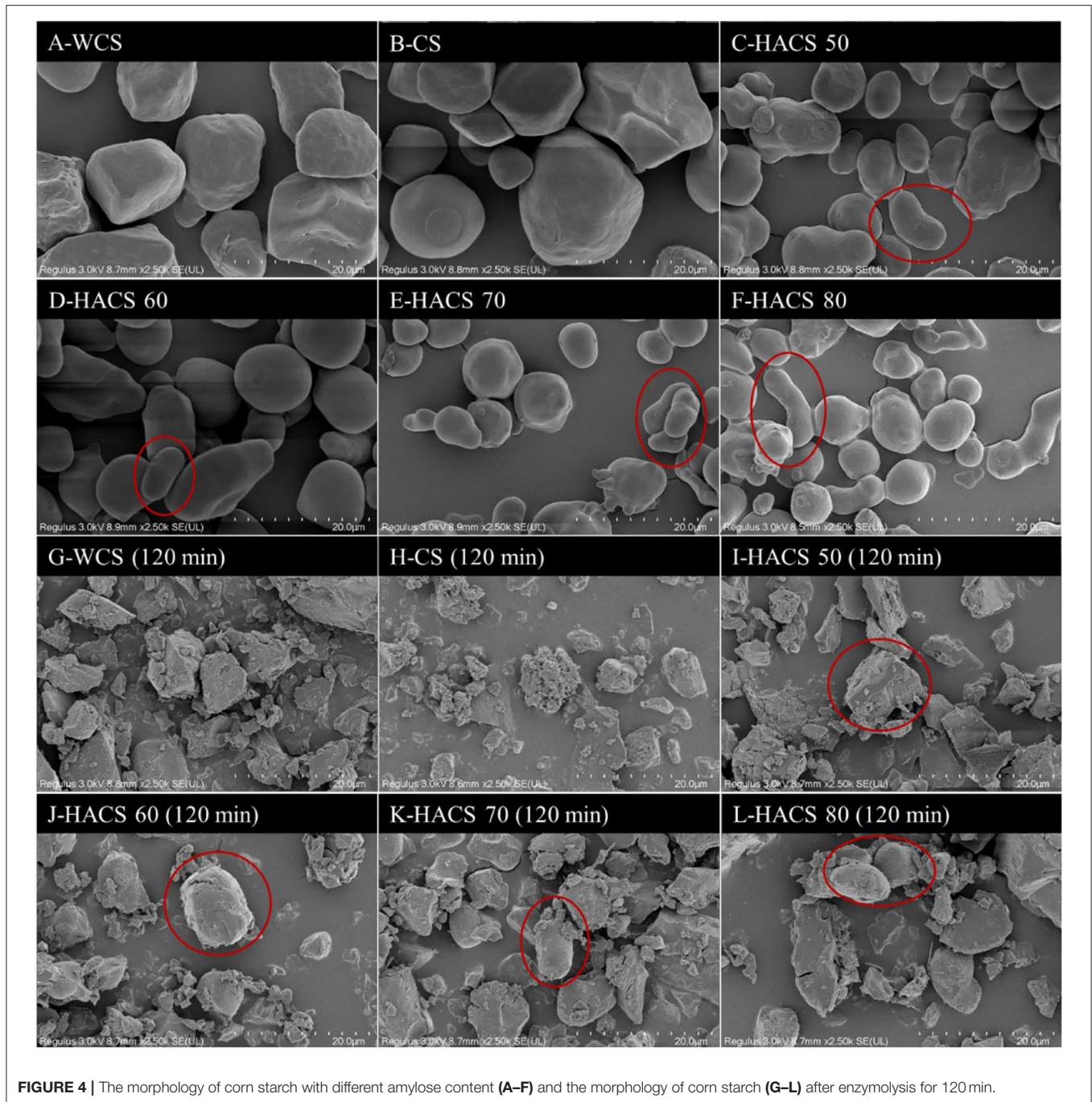


**FIGURE 4 |** The morphology of corn starch with different amylose content (A–F) and the morphology of corn starch (G–L) after enzymolysis for 120 min.

presence of long-chain double helix microcrystals derived from amylose and intermediate components (IC) that stabilize the starch structure (38).

## Thermal Properties

Values corresponding to various thermodynamic properties of corn starch with different amylose content are presented in **Table 3**. DSC results demonstrated that the onset (initial) gelatinization temperature ( $T_o$ ), peak gelatinization temperature ( $T_p$ ), and conclusion (termination) temperature ( $T_c$ ) of HACS

were significantly delayed, and the gelatinization temperature range ( $T_c - T_o$ ) increased significantly. These results concur with those reported for WCS (39). The inner area of starch granules mainly comprises loosely packed amylopectin growth rings with semi-crystalline flakes, which are fragile under gelatinization or hydrolysis (40), therefore, as the content of amylopectin decreased, the gelatinization enthalpy ( $\Delta H$ ) of HACS increased, the maximum  $\Delta H$  was 18.24 J/g. Comparing the content of resistant starch in **Table 1**, the study found that with the increase in RS content, the  $T_o$ ,  $T_p$ ,  $T_c$ , and  $\Delta H$  of HACS showed a

**TABLE 3** | Thermodynamic parameters of corn starch with different amylose content.

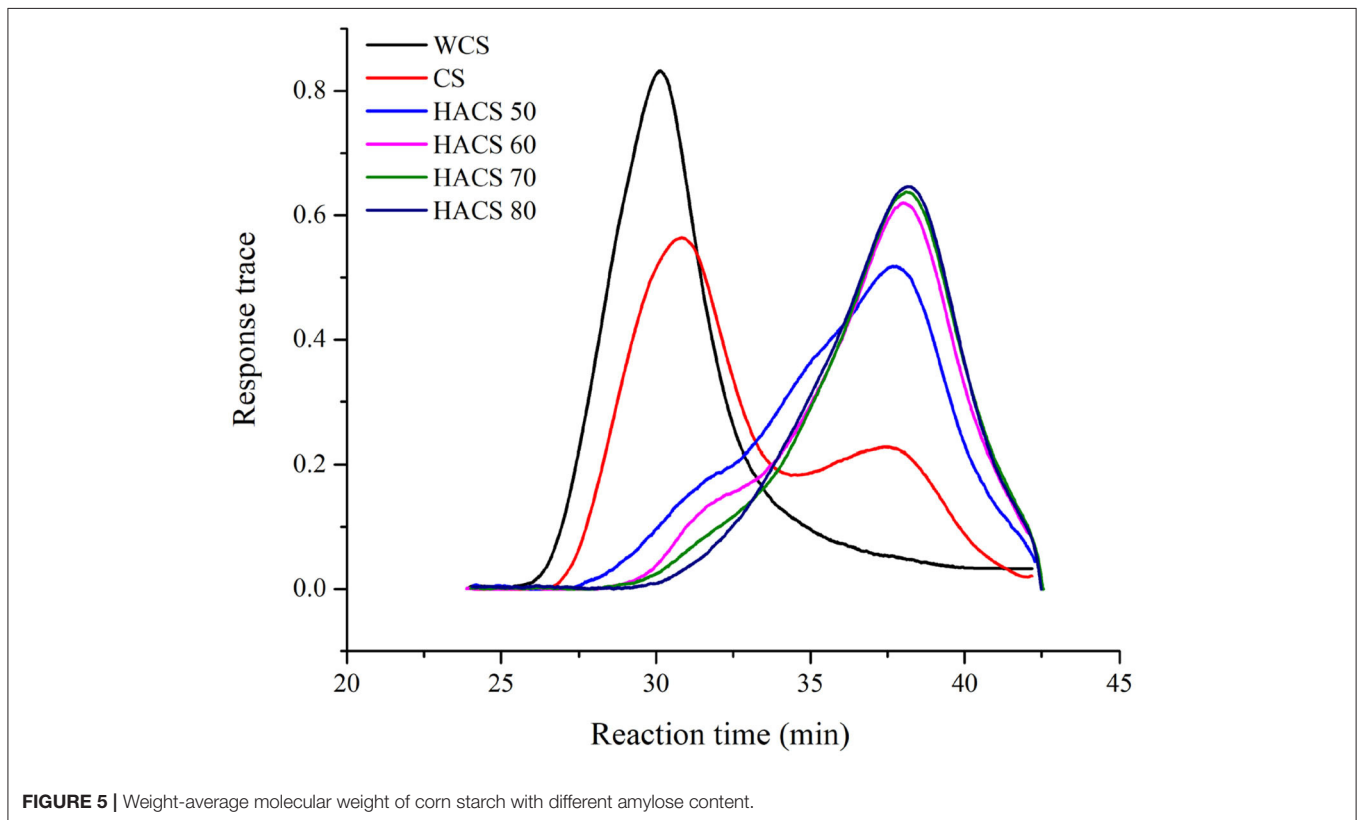
| Samples | $T_o$ (°C)                | $T_p$ (°C)                | $T_c$ (°C)                 | $T_c - T_o$ (°C) | $\Delta H$ (J/g)          |
|---------|---------------------------|---------------------------|----------------------------|------------------|---------------------------|
| WCS     | 67.37 ± 0.05 <sup>c</sup> | 71.56 ± 0.09 <sup>a</sup> | 78.62 ± 0.05 <sup>a</sup>  | 11.25            | 14.54 ± 0.36 <sup>b</sup> |
| CS      | 67.08 ± 0.21 <sup>b</sup> | 71.86 ± 0.17 <sup>b</sup> | 79.05 ± 0.27 <sup>b</sup>  | 11.97            | 13.14 ± 0.12 <sup>a</sup> |
| HACS 50 | 62.55 ± 0.14 <sup>a</sup> | 75.33 ± 0.03 <sup>c</sup> | 103.05 ± 0.16 <sup>c</sup> | 40.50            | 16.86 ± 0.05 <sup>c</sup> |
| HACS 60 | 92.94 ± 0.23 <sup>f</sup> | 95.44 ± 0.14 <sup>e</sup> | 120.73 ± 0.13 <sup>f</sup> | 27.79            | 18.24 ± 0.15 <sup>e</sup> |
| HACS 70 | 76.58 ± 0.12 <sup>d</sup> | 94.06 ± 0.05 <sup>d</sup> | 104.02 ± 0.12 <sup>e</sup> | 27.44            | 17.75 ± 0.13 <sup>d</sup> |
| HACS 80 | 84.49 ± 0.15 <sup>e</sup> | 94.94 ± 0.24 <sup>d</sup> | 106.26 ± 0.17 <sup>d</sup> | 21.77            | 18.05 ± 0.12 <sup>e</sup> |

Values followed by different superscripts in the same column are significantly different ( $p < 0.05$ ).

**TABLE 4** | Debranched chain length distributions and weight-average molecular weight of corn starch with different amylose content.

| Samples | Average chain length      | Branch degree | Amylopectin branch chain length distribution (%) |                           |                           |                           | $M_w$                  |                        |
|---------|---------------------------|---------------|--|---------------------------|---------------------------|---------------------------|------------------------|------------------------|
|         |                           |               | $fa/(fb1 + fb2 + fb3)$                           | $fa$ (%)                  | $fb1$ (%)                 | $fb2$ (%)                 | $fb3$ (%)              | Peak 1                 |
| WCS     | 19.15 ± 0.01 <sup>a</sup> | 0.358         | 26.25 ± 0.09 <sup>f</sup>                        | 51.00 ± 0.21 <sup>d</sup> | 14.97 ± 0.06 <sup>a</sup> | 7.23 ± 0.08 <sup>a</sup>  | 2.23 × 10 <sup>7</sup> | -                      |
| CS      | 19.47 ± 0.02 <sup>b</sup> | 0.339         | 25.14 ± 0.09 <sup>e</sup>                        | 50.58 ± 0.05 <sup>c</sup> | 15.93 ± 0.05 <sup>b</sup> | 7.63 ± 0.07 <sup>b</sup>  | 1.37 × 10 <sup>7</sup> | 2.25 × 10 <sup>5</sup> |
| HACS 50 | 20.50 ± 0.05 <sup>c</sup> | 0.258         | 20.38 ± 0.06 <sup>d</sup>                        | 53.05 ± 0.01 <sup>e</sup> | 16.28 ± 0.27 <sup>c</sup> | 9.50 ± 0.03 <sup>c</sup>  | 1.11 × 10 <sup>7</sup> | 4.28 × 10 <sup>5</sup> |
| HACS 60 | 20.74 ± 0.04 <sup>d</sup> | 0.257         | 20.10 ± 0.08 <sup>c</sup>                        | 50.45 ± 0.47 <sup>c</sup> | 17.82 ± 0.03 <sup>d</sup> | 10.14 ± 0.04 <sup>d</sup> | 5.94 × 10 <sup>6</sup> | 2.59 × 10 <sup>5</sup> |
| HACS 70 | 22.51 ± 0.09 <sup>e</sup> | 0.215         | 17.46 ± 0.04 <sup>a</sup>                        | 47.82 ± 0.17 <sup>b</sup> | 19.24 ± 0.05 <sup>e</sup> | 14.17 ± 0.07 <sup>e</sup> | -                      | 6.42 × 10 <sup>5</sup> |
| HACS 80 | 22.85 ± 0.04 <sup>f</sup> | 0.225         | 17.90 ± 0.04 <sup>b</sup>                        | 45.44 ± 0.05 <sup>a</sup> | 19.10 ± 0.02 <sup>e</sup> | 15.02 ± 0.10 <sup>f</sup> | -                      | 5.03 × 10 <sup>5</sup> |

Values followed by different superscripts in the same column are significantly different ( $p < 0.05$ ).

**FIGURE 5** | Weight-average molecular weight of corn starch with different amylose content.

consistent increasing trend, which indicates that the RS content of starch is closely related to the thermal stability of starch. Besides amylose content, starch digestibility is still affected by

the orderly spiral structure between amylose molecules (41). The orderly arrangement of amylose could increase the stability of starch granules and improve heat resistance. HACS 60 had the

highest RS content (49.10%) and the highest  $\Delta H$ , proving that it has a more ordered spiral structure between amylose molecules.

### Debranched Chain Length Distributions

According to existing report (42), the debranched chain segment can be divided into four parts. As shown in **Table 4**, as the apparent amylose content increases, the average chain length of starch and the degree of branching increases (43), the maximum average chain length is 22.85 and the minimum branching degree is 0.215. The high content of long chains ( $fb3$ ,  $DP \geq 37$ ) and low degree of branching [ $fa/(fb1 + fb2 + fb3)$ ] in amylopectin are associated with the digestibility of starch. The long chains in amylopectin can form longer double helices and strengthen the hydrogen bonding force between the chain segments, making the structure more stabilized and increasing the RS content of starch. However, the short branches of amylopectin make the layered structure of the crystal unstable.

### Weight-Average Molecular Weight

**Table 4** shows that as the amylose content increased, the Weight-average molecular weight ( $M_w$ ) of the samples continued to decrease. The maximum and minimum  $M_w$  of the samples were  $2.23 \times 10^7$  and  $5.03 \times 10^5$ , respectively. HACS obviously had a narrow  $M_w$  (**Figure 5**), which characterized the subtle differences between starch molecules and the relatively

uniform molecular size (29). Amylose mainly comprises a linear structure (glucose monomers with  $\alpha$ -1,4-glycosidic bonds) and several long branches. According to existing research, during the digestion process, the long straight chains of CS are broken into short straight chains, and the original RS content of the starch can be increased through the formation of more double helices (43). A large amount of amylose in HACS easily produces a similar structure during digestion, which may be an important reason why HACS has a high RS content.

### Crystal Structure

**Figure 6** shows the X-ray diffraction (XRD) pattern and relative crystallinity of corn starch with different amylose content. The crystal structure of starch can be attributed to the accumulation of amylopectin side chains forming a double helix (44), which can be divided into A, B, and C types; HACS belongs to type B starch. The relative crystallinity of HACS is lower than WCS and CS, and as the content of amylose increases, the relative crystallinity gradually decreases. Compared with type A starch, the content of  $fa$  (DP6-12) was lower, and the content of  $fb3$  ( $DP \geq 37$ ) was higher, which is consistent with the results in **Table 4**. It can be seen that the crystal structure does not promote the increase of RS content.

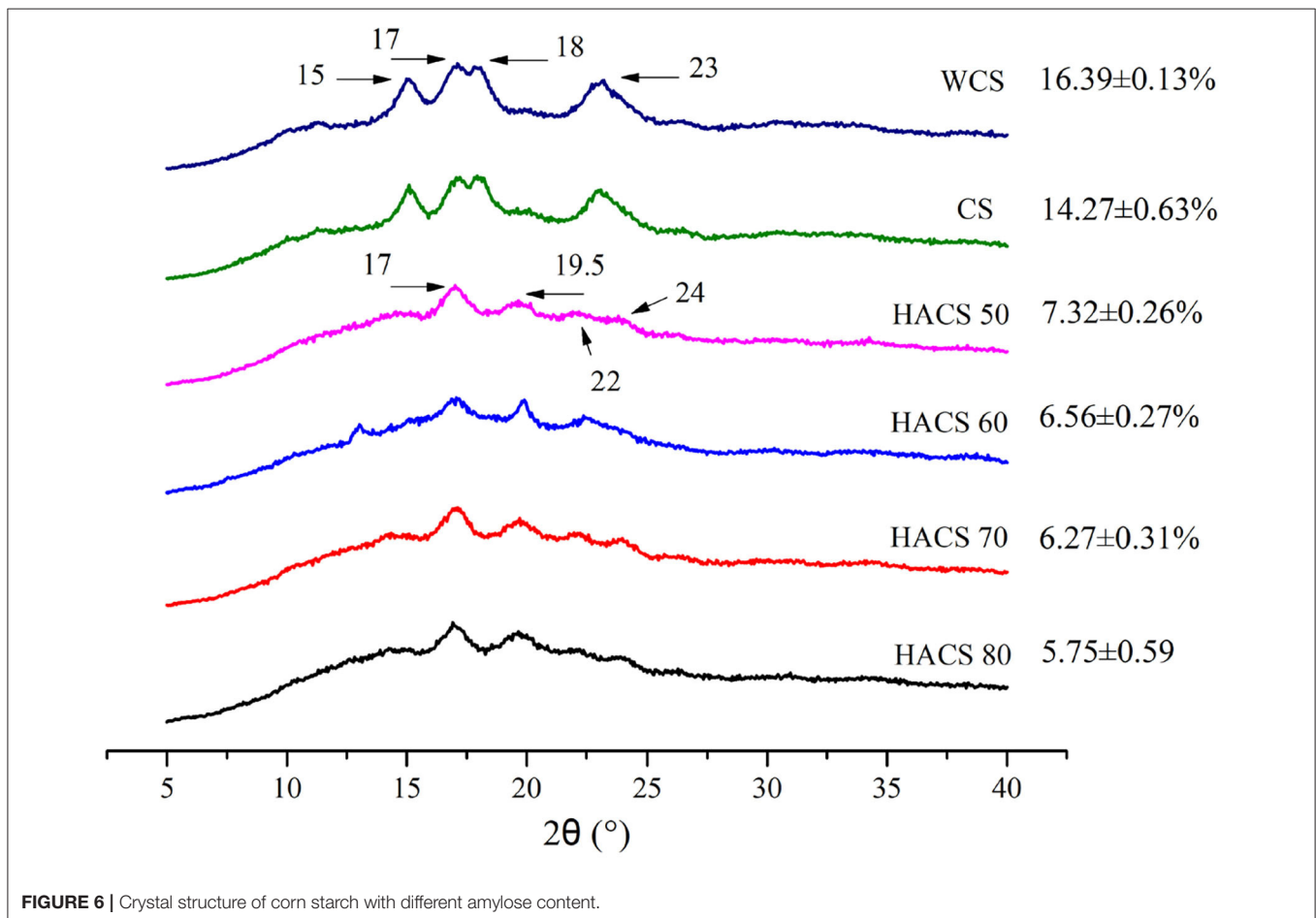


**FIGURE 6** | Crystal structure of corn starch with different amylose content.

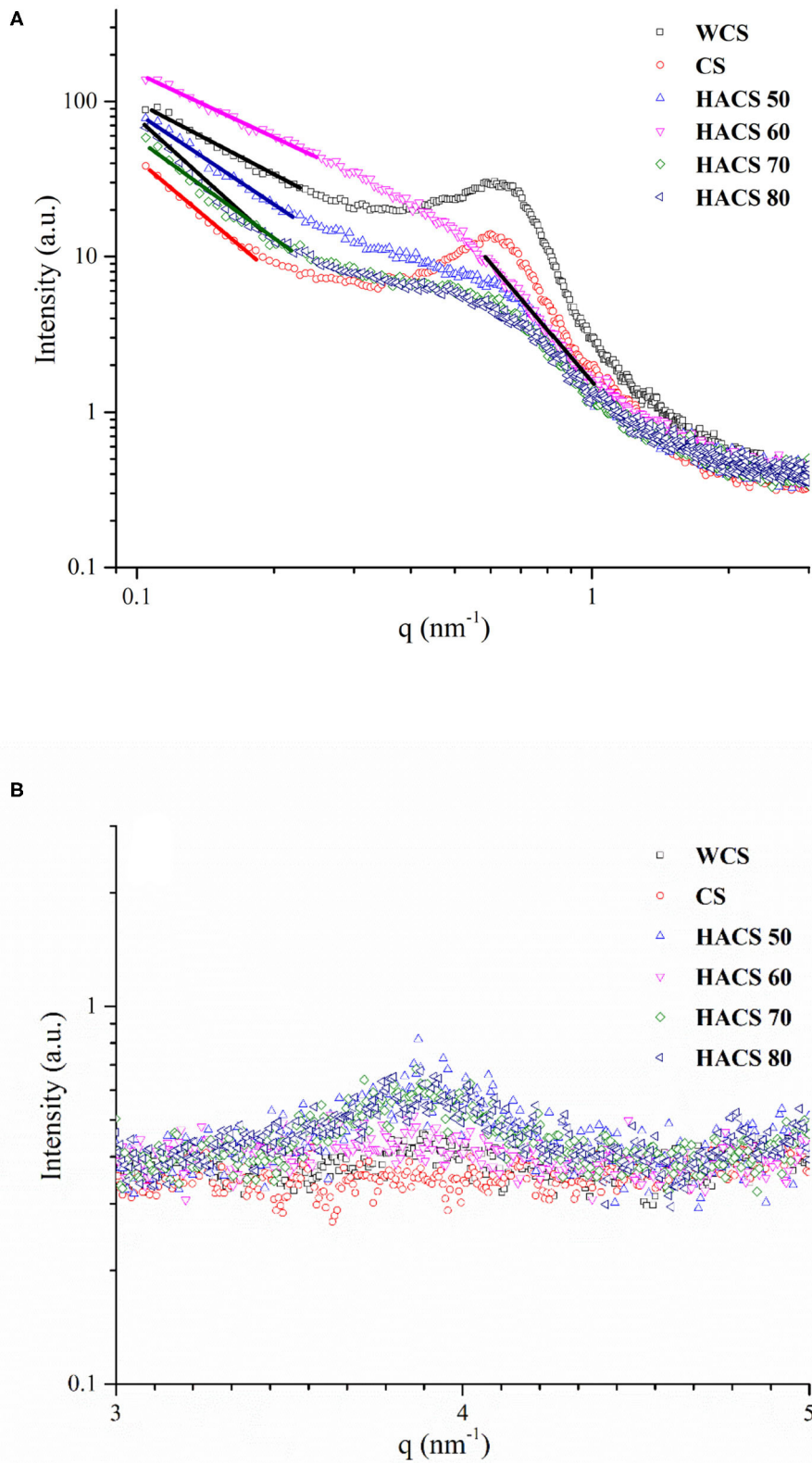


**FIGURE 7** | Double-logarithmic SAXS patterns (A), log I-q SAXS patterns (B).

**TABLE 5** | SAXS parameters of different samples.

| Samples | $q$ (nm <sup>-1</sup> ) | $d_1$ (nm) | $\alpha_1$ | $D_{m1}$ | $\alpha_2$ | $D_{s2}$ |
|---------|-------------------------|------------|------------|----------|------------|----------|
| WCS     | 0.6130                  | 10.24      | 1.07       | 1.07     | –          | –        |
| CS      | 0.6000                  | 10.47      | 1.01       | 1.01     | –          | –        |
| HACS 50 | 0.5908                  | 11.20      | 1.28       | 1.28     | –          | –        |
| HACS 60 | –                       | –          | 1.44       | 1.44     | 3.54       | 2.46     |
| HACS 70 | 0.5935                  | 10.58      | 1.11       | 1.11     | –          | –        |
| HACS 80 | 0.5869                  | 10.70      | 1.16       | 1.16     | –          | –        |

## Fractal Structure

The double logarithmic SAXS pattern of corn starch with different linear contents is shown in **Figure 7A**. According to the scattering power law equation:  $I = q^{-\alpha}$ , where  $I$  is the SAXS intensity and  $\alpha$  is the index which can calculate the  $D$  value of the surface/mass fractal structure, and can be obtained from the slope of the log-log SAXS diagram. When  $1 < \alpha < 3$ , the scatterer is a mass fractal, which is relatively loose. For fractal index  $D_m = \alpha$ , the closer  $D_m$  is to 1, the looser it is, and the closer to 3 the denser; when  $3 < \alpha < 4$ , the scatterer is a surface fractal. Relatively dense, rough surface, the fractal index  $D_s = 6 - \alpha$  is generally between 2 and 3. The closer  $D_s$  is to 2, the smoother the surface, whereas the closer to 3, the rougher the surface. According to the Woolf-Bragg formula  $d = 2\pi/q$ , the scattering peak of about  $0.6 \text{ nm}^{-1}$  in the SAXS curve can calculate the semi-crystalline layer thickness  $d$  of starch granules. The scattering object of the surface fractal is more compact than the scattering object of the mass fractal.

HACS 60 has a shoulder-like structure at  $q = 0.2\text{--}0.4 \text{ nm}^{-1}$ , which may be caused by the tight rearrangement of amylose (45), which may have been likely because it had two fractal-scattering regions at high and low  $q$  values, with different fractal dimensions. According to fractal geometry, scattering patterns with multiple power law regions can indicate the unique structural characteristics of materials at different length scales (46). As presented in **Figure 7A** and **Table 5**, all samples belong to the mass fractal. Samples WCS ( $D_{m1} = 1.07$ ) and CS ( $D_{m1} = 1.01$ ) were characterized between  $17.20 < d(2\pi/q) < 43.77 \text{ nm}$ . HACS 50 ( $D_{m1} = 1.28$ ), HACS 70 ( $D_{m1} = 1.11$ ), and HACS 80 ( $D_{m1} = 1.16$ ) were characterized between  $17.20 < d(2\pi/q) < 37.04 \text{ nm}$ . HACS 60 ( $D_{m1} = 1.44$ ) was characterized between  $12.67 < d(2\pi/q) < 57.09 \text{ nm}$ . These data indicate that the scattering objects in HACS 60 samples are more compact and the mass fractal structure is formed in a large range. Interestingly, for HACS 60, the surface fractal structure is observed to be between  $\sim 7.41 < d$

$(2\pi/q) < 10.58 \text{ nm}$ , and the fractal dimension  $D_{s2} = 2.46$ , which indicates that the scattering objects at the lower scale level are dense and smooth surfaces. As shown in **Figure 7B** HACS has a diffraction peak around  $q = 3.5$ , which is a unique phenomenon of type B crystals (47). This follows the phenomenon observed shown in XRD analysis.

## CONCLUSION

In this study, we determined the *in vitro* digestibility of corn starch with different amylose content. In addition, the factors affecting digestibility were discussed, including particle morphology, debranched chain fine structure, molecular structure, and semi-crystalline structure. The results showed that the higher the amylose content, the higher the RS content. The lower the  $fa$  content, the higher the  $fb2$  and  $fb3$  content, and the more stable the starch structure, the higher the RS content. In addition to amylose content, the arrangement of amylose also has an important influence on RS content. In the quality fractal, the larger the  $D_m$ , the higher the RS content. The shoulder structure is the special structural factor contributing to the highest resistance of HACS 60, and the dense surface fractal is also one of the biggest factors for resistance in starch. Understanding the relationship between the structural factors affecting HACS resistance and RS content will help us to further cultivate corn starch with specific RS content.

## DATA AVAILABILITY STATEMENT

The original contributions generated for the study are included in the article/supplementary material, further inquiries can be directed to the corresponding author/s.

## AUTHOR CONTRIBUTIONS

XL: experimental arrangement and writing. YH: conceptualization, methodology, and supervision. QZ and CJ: analysis and literature review.

## FUNDING

This research was financially supported by the National Natural Science Foundation of China (Nos. 31571794 and 31960456), Qingdao Special Food Research Institute Program (No. 66120005), National First-class Discipline Program of Food Science and Technology (JUFSTR20180204), Guangxi Science and Technology Major Project guikeAA17202029.

## REFERENCES

- Rincon-Londono N, Vega-Rojas LJ, Contreras-Padilla M, Acosta-Osorio AA, Rodriguez-Garcia ME. Analysis of the pasting profile in corn starch: structural, morphological, and thermal transformations, part I. *Int J Biol Macromol.* (2016) 91:106–14. doi: 10.1016/j.ijbiomac.2016.05.070
- Waterschoot J, Gomand SV, Fierens E, Delcour JA. Production, structure, physicochemical and functional properties of maize, cassava, wheat, potato and rice starches. *Starch Stärke.* (2015) 67:14–29. doi: 10.1002/star.201300238
- Englyst HN, Kingman SM, Cummings JH. Classification and measurement of nutritionally important starch fractions. *Eur J Clin Nutr.* (1992) 46:S33–S50.
- Fabek H, Messerschmidt S, Brulport V, Goff HD. The effect of *in vitro* digestive processes on the viscosity of dietary fibres and

- their influence on glucose diffusion. *Food Hydrocolloids*. (2014) 35:718–26. doi: 10.1016/j.foodhyd.2013.08.007
5. Birt DF, Boylston T, Hendrich S, Jane JL, Hollis J, Li L, et al. Resistant starch: promise for improving human health. *Adv Nutr*. (2013) 4:587–601. doi: 10.3945/an.113.004325
  6. Jiang F, Du CW, Jiang WQ, Wang LY, Du SK. The preparation, formation, fermentability, and applications of resistant starch. *Int J Biol Macromol*. (2020) 150:1155–61. doi: 10.1016/j.ijbiomac.2019.10.124
  7. Lin LS, Guo DW, Zhao LX, Zhang XD, Wang J, Zhang FM, et al. Comparative structure of starches from high-amylose maize inbred lines and their hybrids. *Food Hydrocolloids*. (2016) 52:19–28. doi: 10.1016/j.foodhyd.2015.06.008
  8. Li HT, Gidley MJ, Dhital S. High-amylose starches to bridge the “Fiber Gap”: development, structure, and nutritional functionality. *Compr Rev Food Sci Food Saf*. (2019) 18:362–79. doi: 10.1111/1541-4337.12416
  9. Mua JP, Jackson DS. Relationships between functional attributes and molecular structures of amylose and amylopectin fractions from corn starch. *J Agric Food Chem*. (1997) 45:3848–54. doi: 10.1021/jf9608783
  10. Li NN, Guo YB, Zhao SM, Kong JX, Qiao DL, Lin LZ, et al. Amylose content and molecular-order stability synergistically affect the digestion rate of indica rice starches. *Int J Biol Macromol*. (2020) 144:373–9. doi: 10.1016/j.ijbiomac.2019.12.095
  11. Li L, Jiang HX, Campbell M, Blanco M, Jane JL. Characterization of maize amylose-extender (ae) mutant starches. Part I: relationship between resistant starch contents and molecular structures. *Carbohydr Polym*. (2008) 74:396–404. doi: 10.1016/j.carbpol.2008.03.012
  12. Zhang BJ, Li XX, Liu J, Xie FW, Chen L. Supramolecular structure of A- and B-type granules of wheat starch. *Food Hydrocolloids*. (2013) 31:68–73. doi: 10.1016/j.foodhyd.2012.10.006
  13. Chi CD, Li XX, Zhang YP, Chen L, Li L, Wang ZJ. Digestibility and supramolecular structural changes of maize starch by non-covalent interactions with gallic acid. *Food Funct*. (2017) 8:720–30. doi: 10.1039/C6FO01468B
  14. Bendiks ZA, Knudsen KEB, Keenan MJ, Marco ML. Conserved and variable responses of the gut microbiome to resistant starch type 2. *Nutr Res*. (2020) 77:12–28. doi: 10.1016/j.nutres.2020.02.009
  15. Sievert D, Pomeranz Y. Enzyme-resistant starch. I. Characterization and evaluation by enzymatic, thermoanalytical, and microscopic methods. *Cereal Chem*. (1989) 66:342–7.
  16. Dimantov A, Kesselman E, Shimoni E. Surface characterization and dissolution properties of high amylose corn starch-pectin coatings. *Food Hydrocolloids*. (2004) 18:29–37. doi: 10.1016/S0268-005X(03)00039-0
  17. Wang HW, Zhang BJ, Chen L, Li XX. Understanding the structure and digestibility of heat-moisture treated starch. *Int J Biol Macromol*. (2016) 88:1–8. doi: 10.1016/j.ijbiomac.2016.03.046
  18. Patindol J, Gu X, Wang Y-J. Chemometric analysis of the gelatinization and pasting properties of long-grain rice starches in relation to fine structure. *Starch Starke*. (2009) 61:3–11. doi: 10.1002/star.200800022
  19. Park IM, Lbanes AM, Zhong F, Shoemaker CF. Gelatinization and pasting properties of waxy and non-waxy rice starches. *Starch Starke*. (2007) 59:388–96. doi: 10.1002/star.200600570
  20. Luengwilai K, Beckles DM. Structural investigations and morphology of tomato fruit starch. *J Agric Food Chem*. (2009) 57:282–91. doi: 10.1021/jf802064w
  21. Cardoso MB, Westfahl H Jr. On the lamellar width distributions of starch. *Carbohydr Polym*. (2010) 81:21–8. doi: 10.1016/j.carbpol.2010.01.049
  22. Pikus S. Small-angle X-ray scattering (SAXS) studies of the structure of starch and starch products. *Fibres Text Eastern Europe*. (2005) 13:82–6. Available online at: [http://www.fibtex.lodz.pl/53\\_19\\_82.pdf](http://www.fibtex.lodz.pl/53_19_82.pdf)
  23. Li SL, Ward R, Gao QY. Effect of heat-moisture treatment on the formation and physicochemical properties of resistant starch from mung bean (*Phaseolus radiatus*) starch. *Food Hydrocolloids*. (2011) 25:1702–9. doi: 10.1016/j.foodhyd.2011.03.009
  24. Tattiyakul J, Naksriarporn T, Pradipasena P. X-ray diffraction pattern and functional properties of dioscorea hispida dennst starch hydrothermally modified at different temperatures. *Food Bioprocess Technol*. (2012) 5:964–71. doi: 10.1007/s11947-010-0424-3
  25. Zhu J, Li L, Chen L, Li XX. Study on supramolecular structural changes of ultrasonic treated potato starch granules. *Food Hydrocolloids*. (2012) 29:116–22. doi: 10.1016/j.foodhyd.2012.02.004
  26. Englyst HN, Veenstra J, Hudson GJ. Measurement of rapidly available glucose (RAG) in plant foods: a potential *in vitro* predictor of the glycaemic response. *Br J Nutr*. (1996) 75:327–37. doi: 10.1079/BJN19960137
  27. Dai DD, Sun SL, Hong Y, Gu ZB, Cheng L, Li ZF, et al. Structural and functional characteristics of butyrylated maize starch. *LWT Food Sci Technol*. (2019) 112:7. doi: 10.1016/j.lwt.2019.108254
  28. Sun SL, Hong Y, Gu Z, Cheng L, Li ZF, Li CM. An investigation into the structure and digestibility of starch-oleic acid complexes prepared under various complexing temperatures. *Int J Biol Macromol*. (2019) 138:966–74. doi: 10.1016/j.ijbiomac.2019.07.166
  29. Bi Y, Zhang YY, Jiang HH, Hong Y, Gu ZB, Cheng L, et al. Molecular structure and digestibility of banana flour and starch. *Food Hydrocolloids*. (2017) 72:219–27. doi: 10.1016/j.foodhyd.2017.06.003
  30. Liu GD, Gu ZB, Hong Y, Wei HY, Zhang C, Huang S, et al. Effects of molecular interactions in debranched high amylose starch on digestibility and hydrogel properties. *Food Hydrocolloids*. (2020) 101:8. doi: 10.1016/j.foodhyd.2019.105498
  31. Zhou S, Hong Y, Gu ZB, Cheng L, Li ZF, Li CM. Effect of heat-moisture treatment on the *in vitro* digestibility and physicochemical properties of starch-hydrocolloid complexes. *Food Hydrocolloids*. (2020) 104:10. doi: 10.1016/j.foodhyd.2020.105736
  32. Zhang LL, Li XX, Janaswamy S, Chen L, Chi CD. Further insights into the evolution of starch assembly during retrogradation using SAXS. *Int J Biol Macromol*. (2020) 154:521–7. doi: 10.1016/j.ijbiomac.2020.03.135
  33. Noda T, Nishiba Y, Sato T, Suda I. Properties of starches from several low-amylose rice cultivars. *Cereal Chem*. (2003) 80:193–7. doi: 10.1094/CCHEM.2003.80.2.193
  34. Srichuwong S, Jane JL. Physicochemical properties of starch affected by molecular composition and structures: a review. *Food Sci Biotechnol*. (2007) 16:663–74.
  35. Sanders J, Cohen GM. Observation of the optical & chemical properties of starch granules. *Am Biol Teach*. (2019) 81:644–8. doi: 10.1525/abt.2019.81.9.644
  36. Balet S, Guelpa A, Fox G, Manley M. Rapid visco analyser (RVA) as a tool for measuring starch-related physicochemical properties in cereals: a review. *Food Anal Methods*. (2019) 12:2344–60. doi: 10.1007/s12161-019-01581-w
  37. Li CL, Dhital S, Gilbert RG, Gidley MJ. High-amylose wheat starch: structural basis for water absorption and pasting properties. *Carbohydr Polym*. (2020) 245:11. doi: 10.1016/j.carbpol.2020.116557
  38. Jiang H, Campbell M, Blanco M, Jane J-L. Characterization of maize amylose-extender (ae) mutant starches: part II. structures and properties of starch residues remaining after enzymatic hydrolysis at boiling-water temperature. *Carbohydr Polym*. (2010) 80:1–12. doi: 10.1016/j.carbpol.2009.10.060
  39. Yang J, Xie F, Wen W, Chen L, Shang X, Liu P. Understanding the structural features of high-amylose maize starch through hydrothermal treatment. *Int J Biol Macromol*. (2016) 84:268–74. doi: 10.1016/j.ijbiomac.2015.12.033
  40. Pu HY, Chen L, Li L, Li XX. Multi-scale structural and digestion resistibility changes of high-amylose corn starch after hydrothermal-pressure treatment at different gelatinizing temperatures. *Food Res Int*. (2013) 53:456–63. doi: 10.1016/j.foodres.2013.05.021
  41. Srichuwong S, Sunarti TC, Mishima T, Isono N, Hisamatsu M. Starches from different botanical sources I: contribution of amylopectin fine structure to thermal properties and enzyme digestibility. *Carbohydr Polym*. (2005) 60:529–38. doi: 10.1016/j.carbpol.2005.03.004
  42. Peroni-Okita FHG, Simao RA, Cardoso MB, Soares CA, Lajolo FM, Cordenunsi BR. *In vivo* degradation of banana starch: structural characterization of the degradation process. *Carbohydr Polym*. (2010) 81:291–9. doi: 10.1016/j.carbpol.2010.02.022

43. Witt T, Gidley MJ, Gilbert RG. Starch digestion mechanistic information from the time evolution of molecular size distributions. *J Agric Food Chem.* (2010) 58:8444–52. doi: 10.1021/jf101063m
44. Cheetham NWH, Tao LP. Variation in crystalline type with amylose content in maize starch granules: an X-ray powder diffraction study. *Carbohydr Polym.* (1998) 36:277–84. doi: 10.1016/S0144-8617(98)00007-1
45. Suzuki T, Chiba A, Yano T. Interpretation of small angle X-ray scattering from starch on the basis of fractals. *Carbohydr Polym.* (1997) 34:357–63. doi: 10.1016/S0144-8617(97)00170-7
46. Chavan SV, Sastry PU, Tyagi AK. Fractal and agglomeration behavior in Gd and Sm doped CeO<sub>2</sub> nano-crystalline powders. *J Alloy Compd.* (2008) 457:440–6. doi: 10.1016/j.jallcom.2007.02.140
47. Zhang BJ, Chen L, Zhao Y, Li XX. Structure and enzymatic resistivity of debranched high temperature-pressure treated high-amylose corn starch. *J Cereal Sci.* (2013) 57:348–55. doi: 10.1016/j.jcs.2012.12.006

**Conflict of Interest:** The authors declare that the research was conducted in the absence of any commercial or financial relationships that could be construed as a potential conflict of interest.

Copyright © 2021 Lv, Hong, Zhou and Jiang. This is an open-access article distributed under the terms of the Creative Commons Attribution License (CC BY). The use, distribution or reproduction in other forums is permitted, provided the original author(s) and the copyright owner(s) are credited and that the original publication in this journal is cited, in accordance with accepted academic practice. No use, distribution or reproduction is permitted which does not comply with these terms.